A new route to graphene layers by selective laser ablation

S. Dhar,[1,2,a] A. Roy Barman,[1,3] G. X. Ni,[3] X. Wang,[1,3] X. F. Xu,[3] Y. Zheng,[3] S. Tripathy,[4] Ariando,[1,3] A. Rusydi,[1,3] K. P. Loh,[1,5] M. Rubhausen,[6] A. H. Castro Neto,[3,7] B. Özyilmaz,[1,3] and T. Venkatesan[1,2,3,a]

[1]*NUSNNI NanoCore, National University of Singapore, 117576, Singapore*
[2]*Department of Electrical and Computer Engineering, 117576, Singapore*
[3]*Department of Physics, National University of Singapore, 117542, Singapore*
[4]*IMRE, A*STAR, 117602, Singapore*
[5]*Department of Chemistry, National University of Singapore, 117576, Singapore*
[6]*Institut für Angewandte Physik, Universität Hamburg, D-20355, Hamburg, Germany and Center for Free Electron Laser Science (CFEL), D-22607 Hamburg, Germany*
[7]*Department of Physics, Boston University, Boston MA, 02215, USA*

(Received 5 January 2011; accepted 14 March 2011; published online 20 April 2011)

Selectively creating regions of spatially varying thickness may enable the utilization of the electronic properties of N-layer (N=1 or more) graphene and other similar layered materials (e.g., topological insulators or layered superconductors) for novel devices and functionalities on a single chip. The ablation threshold energy density increases dramatically for decreasing layer numbers of graphene originating from the dimensional crossover of the specific heat. For the 2D regime of graphite (up to N≈7) the dominant flexural mode specific heat (due to its N^{-1} dependence) gives rise to a strong layer number-dependence on the pulsed laser ablation threshold energy density, while for 3D regime (N>>7) the ablation threshold saturates due to dominant acoustic mode specific heat. As a result, several energy density windows exist between the minimum energy densities that are required for ablating single, bi, or more layers of graphene, allowing layer number selectivity. [doi:10.1063/1.3584204]

Graphene, which is a single-layer of carbon atoms, is one of the most fascinating materials, and its extraordinary quantum electronic properties have been recently demonstrated.[1,2] Electrons in this two-dimensional crystal can be described by Dirac's equation,[3] are fully relativistic, and exhibit extremely high mobilities.[4] Moreover, bi-layer graphene allows the fabrication of a field-effect transistor with electric-field-tunable band gap.[5] Despite these attractive properties, the most significant challenge to using this material in devices is the production of defect-free, large-area, single-crystal graphene in a reproducible manner. In addition, a technique to spatially and selectively ablate regions of multi-layer graphene will enable us to exploit the thickness-dependent properties of graphene, such as the utilization of high carrier mobilities (seen in single-layer graphene), a variable band gap (seen in bi-layers), or better ohmic contacts (seen in graphite). Also using this technique, the realization of an all graphene/graphite-based integrated circuit, wherein the many attractive properties of the different manifestations of graphene may be fully exploited. Such a futuristic graphene integrated circuit (not to scale) using highly ordered pyrolytic graphite (HOPG) is shown in Fig. 1.

Currently, the growth of grapheme is dominated by the Cu-based CVD process which allows for the growth of large-area, polycrystalline, single-layer graphene.[6] However, CVD-grown graphene, despite its large area, is polycrystalline due to mosaicity, and the grain sizes are in the sub-millimeter

[a]Authors to whom the correspondence should be addressed. Electronic mail: eleds@nus.edu.sg (S.D.), venky@nus.edu.sg (T.V.).

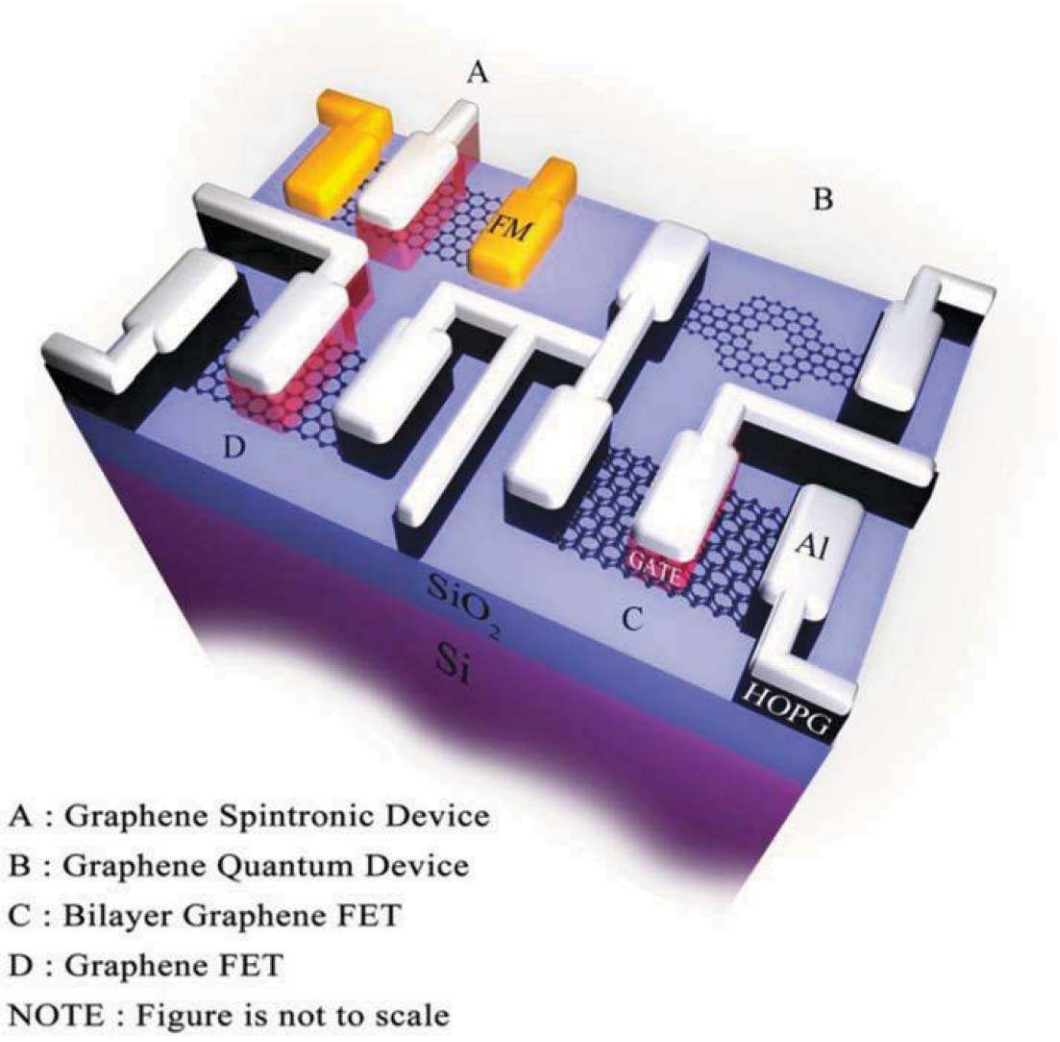

FIG. 1. A futuristic graphene integrated circuit (not to scale), wherein the desirable properties of various thicknesses of graphene layers are utilized along with strategic oxides (SiO_2, ferroelectric, ferromagnetic, multiferroic, etc.) in response to various external stimuli, such as electric or magnetic fields. In the present illustration, the device structure is fabricated from a very thin single-crystal graphite sheet after subsequent patterning/selective ablation. The remaining graphite acts as a good ohmic contact and interconnection between the top Al metallization (which also acts as a self-aligned mask, protecting the underlying graphite) and the variable-thickness graphene-based devices.

range. Moreover, millimeter-sized grains can only occasionally be obtained; hence, a clean *single-crystal* layer of graphene that can be produced on a large scale has yet to be reproducibly achieved. Much larger single crystal graphene on a mm scale could potentially be produced from single crystal graphite using the findings described in this paper, wherein we demonstrate a nsec laser-based process that discriminates between different graphene layer thicknesses. This article presents fundamental experimental data that validate these concepts and reveals an interesting dimensional cross over in the ablation properties of these layers arising from the different nature of the phonon modes in 2 and 3 dimensions.

For present experiments, Graphene flakes of about 5-50μmx5-30 μm in dimension, which were produced by an exfoliation method, were placed on 290-nm-thick SiO_2 films that had been grown on Si substrates. Samples were divided into five groups according to their thicknesses: single layers, bi-layers, 3-5 layers, 5-10 layers, and more than 10 layers. The thickness of the single and bilayers were clearly verified by Raman to 100% accuracy as described by Ferrari *et al.*.[7] The thicker ones which show a larger uncertainty were estimated by an optical color contrast technique and these

measurements give reasonably reproducible values with an increasing uncertainty with N. Then they were ablated by a single pulse of 248 nm (20 nsec) pulsed laser energy at a density of 0.1-1 J/cm^2 at room temperature (RT) in vacuum or an Ar atmosphere or in air. It may be noted that the SiO_2 substrate has little absorption at 248 nm, and the silicon that absorbs at a depth of 290 nm should not play an appreciable role in the heat transfer process. Hydrocarbons and moisture at the interface could play a role, but we treated the samples with a low-energy density, single-shot pulse ($\sim$0.05 J/cm^2), which removed any variability from this interface layer. After laser treatment, the samples were characterized again by both optical and Raman spectroscopy. Standard e-beam lithography and subsequent Cr/Au (5 nm/35 nm) deposition were used to form graphene devices for four terminal measurements.

To determine the optical absorption length, high-energy optical study was done on graphene that was produced from 6H-SiC. The thickness of the graphene layers was determined by Raman spectroscopy and STM. For larger N, we used a technique that was reported by Shivaraman *et al*..[8] The optical absorption of various graphene layers was measured using a spectroscopic generalized ellipsometer (SGE).[9] The experiments were conducted under an ultra-high vacuum condition of 5x10^{-9} mbar in order to ensure that there was no surface contamination during the measurements. The SGE is a unique spectroscopic technique because, from one single measurement, the dielectric function ($i^*\varepsilon_1 + \varepsilon_2$) as well as the absorption coefficient can be obtained without performing the Kramers-Kronig transformation.

To illustrate the dramatic thickness dependence of the ablation process we compare a single layer grapheme with a multilayer sample. Figure 2(a) depicts an optical microscope image of a pristine single-layer graphene flake (5 μm x10 μm), and the corresponding Raman spectrum is shown in Fig. 3. The Raman spectrum clearly depicts the presence of a sharp G peak at 1596 cm^{-1} and a 2D peak at 2708 cm^{-1}. A multi-layer graphene flake of varying thickness (approximately 5-30 layers as determined by color contrasts under optical microscope) was also placed near the single-layer graphene. Both flakes were irradiated with a single pulse (248 nm, 20 ns) of laser energy at a density of 0.1-1 J/cm^2 at room temperature (RT) in Ar atmosphere, and the results are depicted in Fig. 2(b)–2(d).

It is clear from Fig. 2(b) that both the layers are not appreciably affected at 0.1 J/cm^2; however, the Raman spectrum depicted in Fig. 3 demonstrates that the intensities of the G and 2D peaks of the single-layer graphene slightly decrease, while a D peak (in the inset) at 1350 cm^{-1} appears. The D peak indicates the presence of defects; however, at an energy density of 0.2 J/cm^2, most of the layers from the thicker flake are ablated (Fig. 2(c)), but not the single-layer graphene. Only a further decrease in intensity of the 2D peak and an increase in the intensity of the D signal are observed. This trend continues as a function of increasing energy density (Fig. 2(d)), and finally, the ablation threshold energy density (E_{th}) for single-layer is found to be $\sim 0.85 \pm 0.1$ J/cm^2.

Similar to the single-layer graphene, the bi-layer graphene (as verified by Raman spectroscopy, not shown here) was unaffected up to 0.5 J/cm^2 and E_{th} was observed to be $\sim 0.55 \pm 0.1$ J/cm^2. Laser ablations that were conducted in vacuum show similar behaviors as those in Ar, whereas laser ablations in air oxidize the graphene layers and hence, this process is most suited for inert or vacuum ambient.

Fig. 4 summarizes the results of the ablation of various graphene layers as a function of laser ablation energy density. All thicker layers (>3-5 layers) can be observed to have been ablated using fluences of less than or equal to 0.6 J/cm^2. Clearly, there is a significant difference in the E_{th} for single (0.85 J/cm^2) and bi-layer (0.55 J/cm^2) graphene, which rapidly decreases with an increasing number of graphene layers.

What is the origin of this strong layer-number dependence of E_{th}? This must be from the two fundamental properties (optical absorption coefficient and specific heat) of N-layer graphene which play important roles in determining the E_{th}. The laser spot ($\sim$mm) is much bigger than the sample ($\sim$tens of micron) and due to the thermal boundary resistance the role of thermal conductivity can be neglected in the heat equation.

We first focus on the optical absorption data (experimental details in online materials) in Fig. 5 in which the optical absorption length, α^{-1} (normalized by N=1), at $\sim$5 eV ($\sim$248 nm) is depicted as a function of the graphene layer-number N and can be approximated as N$^{-0.38}$. The inset of

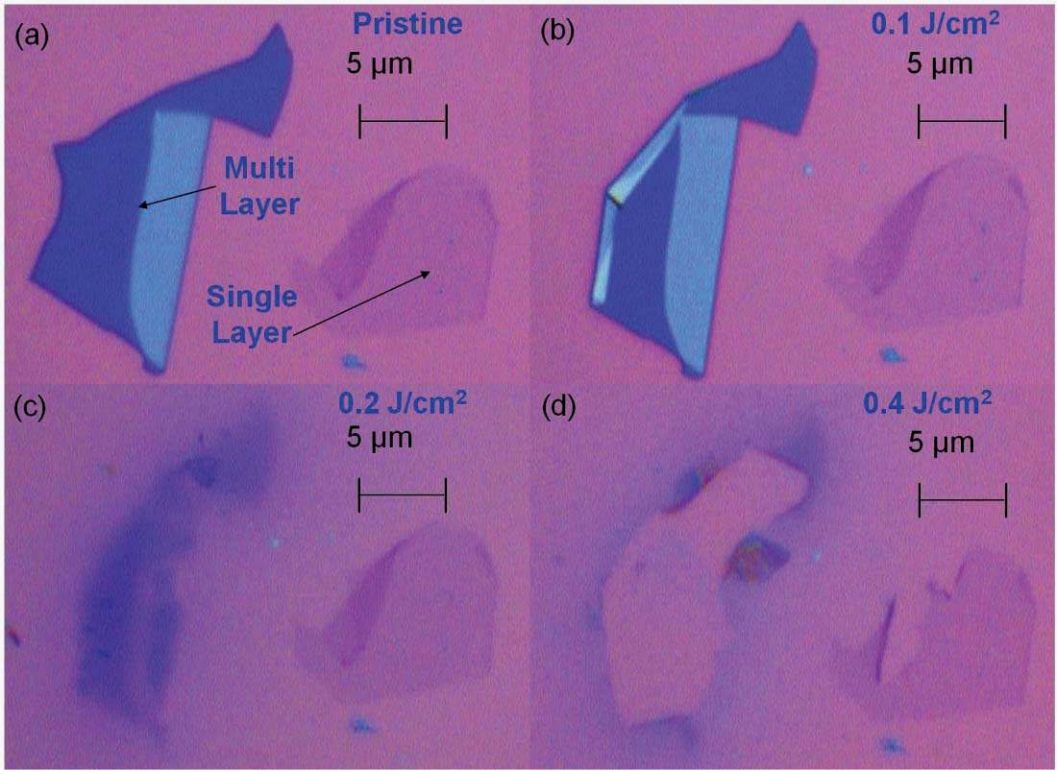

FIG. 2. The laser irradiation-induced effects on a single and multilayer graphene at RT in Ar atmosphere: (a) pristine (b) 0.1 J/cm^2 (c) 0.2 J/cm^2 (d) 0.4 J/cm^2.

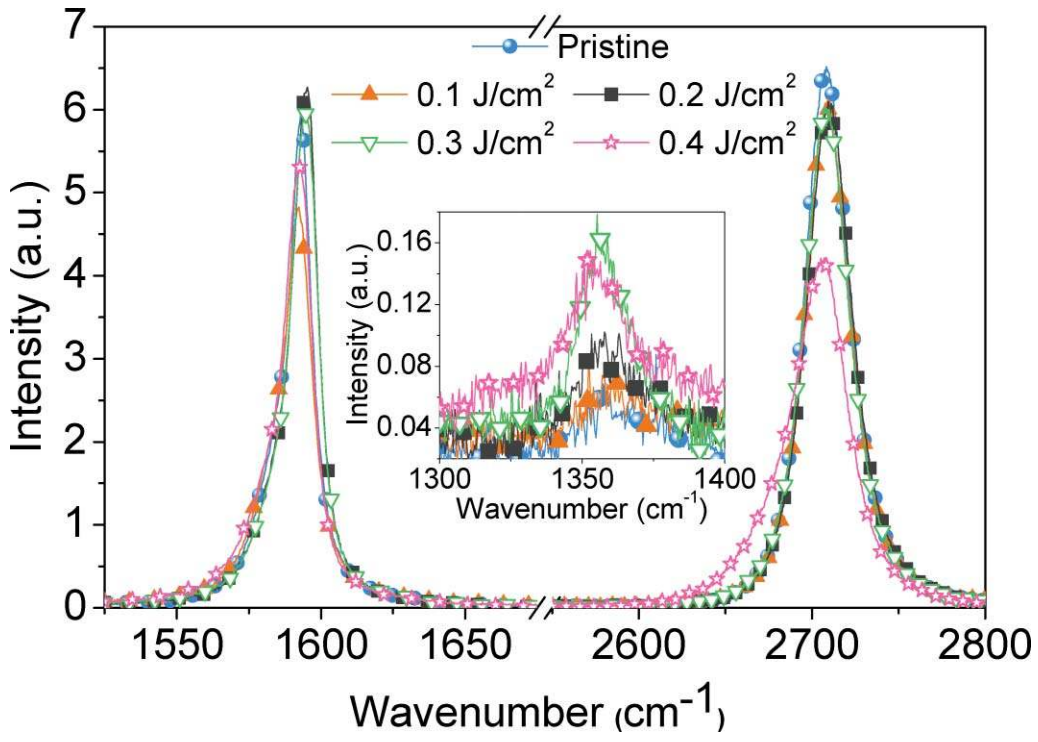

FIG. 3. Raman spectra of the laser irradiated graphene samples whose images are displayed in Fig. 1(a)–1(d), showing G, 2D, and D (in the inset) peaks.

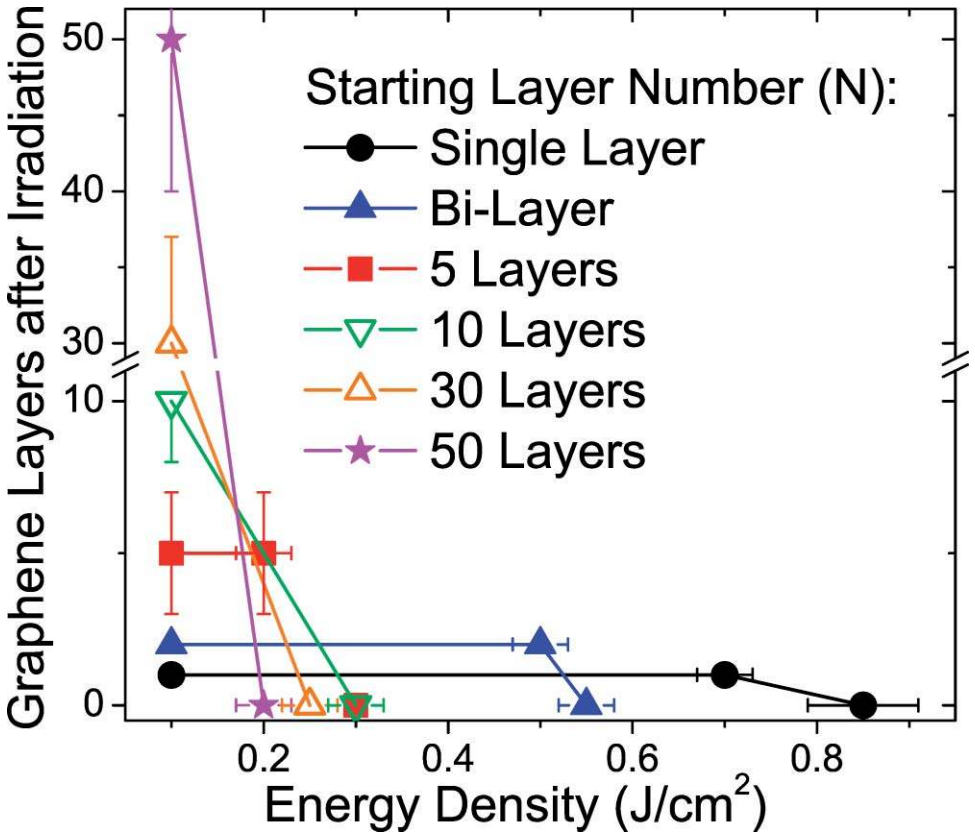

FIG. 4. The ablation of graphene layers as a function of laser energy density and graphene layer-number N clearly showing the existence of the differences in E_{Th} between single-, bi-or more layers.

Fig. 5 depicts α as a function of incident photon energy on various graphene layer thicknesses. Fig 6 shows a plot of threshold energy density versus layer numbers where for each data point shown, the thickness and ablation threshold data for a number of samples ranging from 3-6 was averaged and shown as a single data point with error bars. As shown (red solid line). the optical absorption alone is incapable of adequately explaining the large variation of E_{th} with N.

Hence, this N dependence of E_{th} is most likely due to how the heat couples with the N-layer graphene or graphite via phonons in order to raise its temperature. The nature of the phonon contribution to the specific heat as a function of N is very important. In layered systems, "flaking" occurs because out-of-plane (flexural) modes "melt" the weak interlayer interaction. In single-layer graphene, these flexural modes can be excited with a laser beam,[10] and for an N-layer system, the flexural mode dispersion is given by:

$$\omega_N(\mathbf{k}) = (Y/\rho)^{1/2} cN\mathbf{k}^2 \quad (1)$$

where $\mathbf{k}$ is the two-dimensional momentum, Y=1 TPa is the Young's modulus of graphite ρ= 2,200 kg/m^3 is the mass density of graphite, and c=0.34 nm is the interlayer distance. Amazingly enough, it has been shown that this dispersion is valid for even N=1, wherein the bending rigidity, κ, of graphene is related to the parameters[3] of graphite by $\kappa = Yc^3 = 1$ eV. Using Eq. (1), it is a simple task to compute the flexural (C_f) contribution to the specific heat of the N-layer system:

$$C_f(N, T) = (\pi/12)(\rho/Y)^{1/2}(k_B{}^2 T/c)N^{-1} \quad (2)$$

where k_B is Boltzmann's constant; hence, the specific heat scales with 1/N. In a macroscopic crystal, wherein N>>1, the flexural modes turn into acoustical out-of-plane modes (C_a) and the dispersion changes to $\omega(k) = vk$, where v is the out-of-plane sound velocity. Figure 6 (green line) depicts a fit to the E_{th} assuming only the N dependence of C_f. It is clear that the fit is not good for N>5.

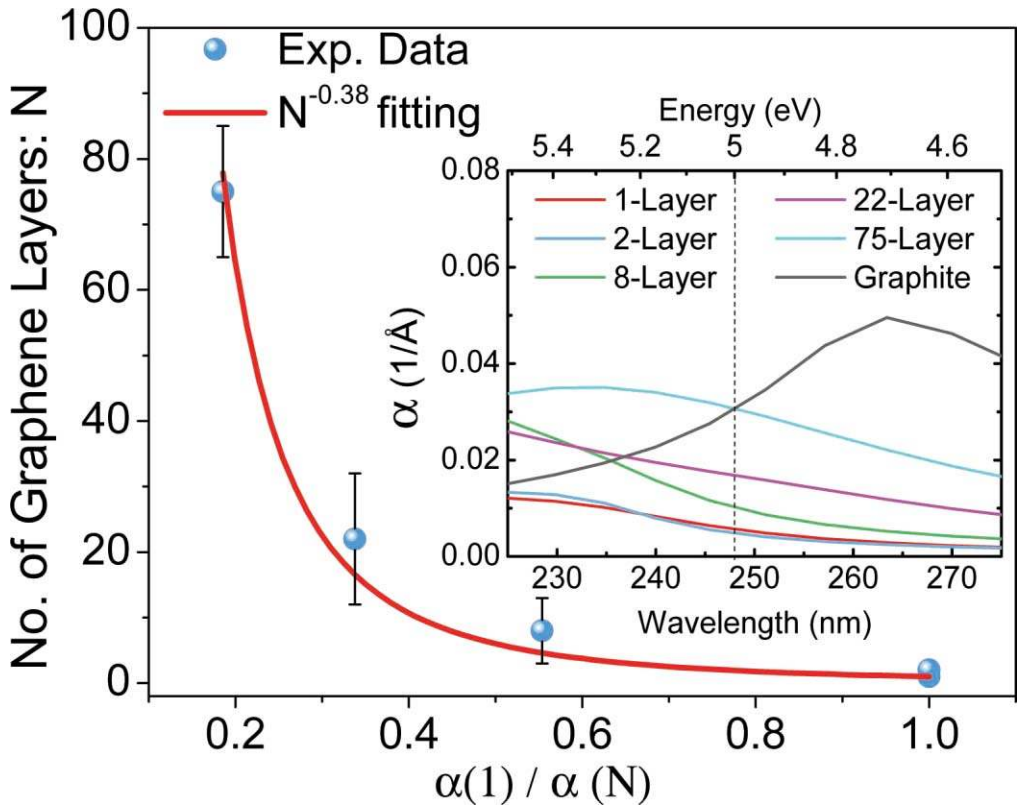

FIG. 5. The graphene layer-number N, as a function of α^{-1} of N-layers (normalized to N = 1), shows an approximate $N^{-0.38}$ dependence at 5 eV. The inset shows α as a function of incident photon energy.

In order to fit this function over the entire range of N values, we will have also to take into account the C_a which dominates in the large N limit. In Fig. 6, we have fitted (blue solid line) the experimental data by assuming that the E_{th} can be approximated by the following energy balance equation (per unit mass):

$$E_{th}(J/cm^2) = C_0 C_t(N, T)/\alpha = C_0 N^{-0.38}(C_f + C_a) = C_0 N^{-0.38}[N^{-1} + (1 - e^{-N/N_0})] \quad (3)$$

where, the total specific heat is $C_t = C_f + C_a$, $\alpha \sim N^{0.38}$, $C_0 = 0.8$ is a constant. A value of $N_0 = 7.4$ is obtained from the best fit and this represents the minimum number of graphene layers that is needed to form a 3D graphite from the perspective of acoustical mode of specific heat. This observation is interesting, especially because this value is consistent with the experimentally measured layer numbers (~5-10), beyond which the Raman signals from the graphene and graphite are indistinguishable.[7] Hence, the existence of the ablation threshold energy gap is a property of 2D graphene, and the decreasing energy gap as a function of increasing layer number is the direct manifestation of the 2D-to-3D transition of graphene to graphite. These results are also consistent with the recent work[11] on the observation of dimensional crossover of thermal conductivity as a function of layer numbers in graphene where the nature of the phonon changes from 2D-to-3D.

To cast this experiment in the light of what has been done with other systems, unlike the case of the nsec laser melting of silicon,[12] wherein the thermal conductivity becomes an integral part of the heat equation, the strong anisotropy of graphite's thermal conductivity enables the above approximation to work. As can be seen, this simple theory agrees well with the experimental data. This result is a consequence of the interplay of phonon dynamics, which strongly depend on the number of layers and manifests only for nsec laser irradiation; however, in many fsec laser studies,[13–15] such a simple dependence has not been observed because the time scales of the dynamics are too fast for phonon kinetics.

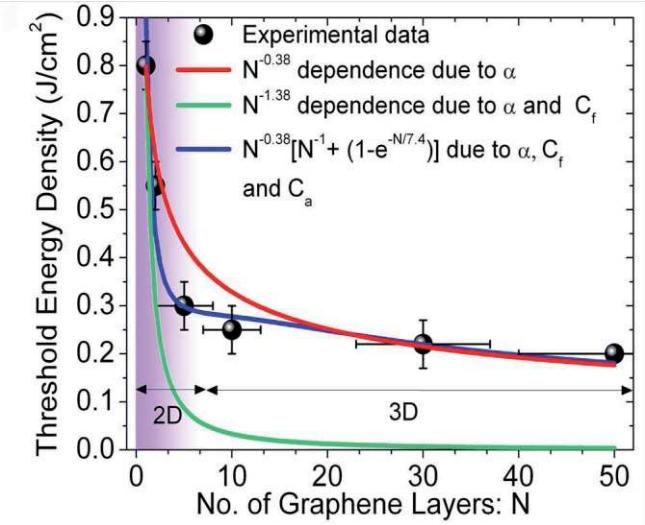

FIG. 6. The ablation threshold energy density (E_{Th}) is plotted as a function of graphene layer-number N. The red solid line is the $N^{-0.38}$ dependence that arises from only α, the green solid line is the $N^{-1.38}$ dependence that arises from both α and flexural mode (C_f) specific heat (Eq. (2)), and the blue solid line with the product of α and total specific heat (Eq. (3)).

In order to understand the usefulness of this process, we fabricated a graphene device (shown in the inset of Fig. 7) that was fabricated from a laser-irradiated single-layer graphene sheet that was subjected to a dose of 0.2 J/cm^2 at RT in Ar. Figure 7 depicts the resistance (R) versus gate voltage (V_{BG}) of this device. Quantitatively, such ambipolar R vs. V_{BG} characteristics can be well fitted by the model[16]:

$$R = \frac{L}{W\mu e\sqrt{n_0^2 + (\alpha(V - V_0))^2}} \tag{4}$$

Where n_0 is the residual carrier density at minimum conductivity, L=6.3 μm, and W=2.2 μm are the length and width of our graphene working channel, $\alpha(V\text{-}V_0)$=n, the carrier concentration induced by back gate bias away from the Dirac point. A rather high field effect mobility (μ) of about 12,000 cm^2/Vs can be extracted from the fitting, with a sheet resistance of approximately 250 Ohms. The present results demonstrate that the laser irradiation used in this work does not negatively impact the electron mobility or resistivity of the graphene, preserving their electronic usefulness for device applications at energy densities of less than 0.2 J/cm^2. An optimized combination of laser wavelength, pulse duration, substrate temperature, and ambient gas could increase this energy density to higher values. Alternatively, by using higher substrate temperatures the ablation energy density could be brought down.

In summary, while this paper successfully shows the underlying science behind the process that is needed to achieve the vision depicted in Fig. 1, it will take further experimental effort to fully realize the potential of this process. The ablation threshold energy density increases dramatically for decreasing layer numbers of graphene originating from the dimensional crossover of the specific heat. For the 2D regime of graphite (up to N≈7) the dominant flexural mode specific heat (due to its N^{-1} dependence) gives rise to a strong layer number-dependence on the pulsed laser ablation threshold energy density, while for 3D regime (N>>7) the ablation threshold saturates due to dominant acoustic mode specific heat and the 2D to 3D cross over occurs close to the values obtained from Raman measurements. As a result, several energy density windows exist between the minimum energy densities that are required for ablating single, bi, or more layers of graphene, allowing layer number selectivity. While it is obvious that one can exploit this process for graphene, this may also be applicable to other important layered structure materials with weak interlayer coupling, such as $MoSe_2$, NbS_2, topological insulators (Bi_2Se_3, Bi_2Te_3, and Sb_2Te_3), and BSCCO superconductors.

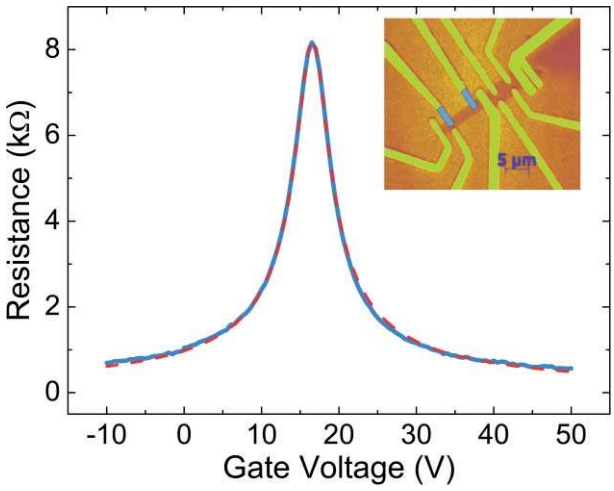

FIG. 7. The four-terminal device resistance (blue solid line) versus gate voltage of a graphene sheet (dotted red line is the fit to Eq. (4)) that has been irradiated at a laser energy density of 0.2 J/cm^2 at RT in Ar atmosphere.

ACKNOWLEDGEMENTS

The authors would like to thank M. Motapothula, I. Santoso, K. K. T., T. C. Tat. This work is supported by grants NRF2008NRF-CRP002-024 and R-143-000-360-281, NRFRF2008-07, NUS YIA, BMBF, U.S. DOE grant DE-FG02-08ER46512 and U.S. Naval Research grant MURI N00014-09-1-1063.

[1] K. S. Novoselov, A. K. Geim, S. V. Morozov, D. Jiang,Y. Zhang, S. V. Dubonos, I. V. Grigorieva, and A. A. Firsov, Science **306**, 666 (2004).
[2] A. K. Geim, Science **234**, 1530 (2009).
[3] A. H. Castro Neto, F. Guinea, N. M. R. Peres, K. S. Novoselov, and A. K. Geim, Rev. Mod. Phys. **81**, 109 (2009).
[4] S. V. Morozov K. S. Novoselov, M. I. Katsnelson, F. Schedin, D. C. Elias, J. A. Jaszczak, and A. K. Geim, Phys. Rev. Lett. **100**, 016602 (2008).
[5] E. V. Castro, K. S. Novoselov, S. V. Morozov, N. M. R. Peres, J. M. B. Lopes dos Santos, J. Nilsson, F. Guinea, A. K. Geim, and A. H. Castro Neto, Phys. Rev. Lett. **99**, 216802 (2007).
[6] X. Li, Y. Zhu, W. Cai, M. Borysiak, B. Han, D. Chen, R. D. Piner, L. Colombo, and R. S. Ruoff, Nano Lett. **9**, 4359 (2009)
[7] A. C. Ferrari, J. C. Meyer, V. Scardaci, C. Casiraghi, M. Lazzeri, F. Mauri, S. Piscanec, D. Jiang, K. S. Novoselov, S. Roth, and A. K. Geim, Phys. Rev. Lett. **97**, 187401 (2006).
[8] S. Shivaraman, M. V. S. Chandrashekhar, J. J. Boeckl, and M. D. Spencer, J. Elec. Mat. **38**, 725 (2009).
[9] R. Rauer, G. Neuber, J. Kunze, J. Bäckström, and M. Rübhausen, Rev. Sci. Instrum. **76**, 023910 (2005).
[10] J. S. Bunch, A. M. Van Der Zande, S, S. Verbridge, I. W. Frank, D. M. Tanenbaum, J. M. Parpia, H. G. Craighead, and P. L. McEuen, Science **315**, 490 (2007).
[11] S. Ghosh, W. Bao, D. L. Nika, S. Subrina, E. P. Pokatilov, C. N. Lau, and A. A. Balandin, Nature Mat. **9**, 555 (2010).
[12] J. M. Poate, and J. W. Mayer, *Laser annealing of semiconductors* (academic, NY, 1982).
[13] H. O. Jeschke M. E. Garcia, and K. H. Bennemann, Phys. Rev. Lett. **87**, 015003 (2001).
[14] M. Lenner, A. Kaplan, and R. E. Palmer, Appl. Phys. Lett. **90**, 153119 (2007).
[15] J. Kanasaki, E. Inami, K. Tanimura, H. Ohnishi, and K. Nasu, Phys. Rev. Lett. **102**, 087402 (2009).
[16] S. Kim, J. Nah, I. Jo, D. Shahrjerdi, L. Colombo, Z. Yao, E. Tutuc, and S. K. Banerjee, Appl. Phys. Lett. **94**, 062107 (2009).